New BIOTECHNOLOGY 89 (2025) 1–10

Contents lists available at ScienceDirect

New BIOTECHNOLOGY

journal homepage: www.elsevier.com/locate/nbt

Tailored enzyme expression modifies *Shewanella oneidensis* biofilms and increases current density

Edina Marlen Klein [a,1], Hannah Heintz [b,2], René Wurst [a,3], Christian Jonas Lapp [a,4], Miriam Edel [a,5], Hendrik Hähl [b,6], Karin Jacobs [b,c,7], Johannes Gescher [a,8,*]

[a] *Institute of Technical Microbiology, University of Technology Hamburg, Hamburg 21073, Germany*
[b] *Experimental Physics, Saarland University, Center for Biophysics, Saarbrücken 66123, Germany*
[c] *Max Planck School Matter to Life, Heidelberg 69120, Germany*

ARTICLE INFO

Keywords:
Biofilm
Microfluidics
Shewanella
Bioelectrochemistry
Optical coherence tomography

ABSTRACT

Biofilm formation is the most effective pathway for electron transfer to anodes in bioelectrochemical systems. However, the mechanisms triggering biofilm formation under anoxic conditions, as well as the architectural and compositional factors that positively influence current generation, are not well understood. Recent findings have shown that riboflavin can function similarly to a quorum sensing molecule in the γ-proteobacterium *Shewanella oneidensis*. Enhanced biofilm formation induced by riboflavin correlates with increased current densities. Only a limited number of candidate proteins were found to have altered concentrations due to this quorum sensing mechanism. This study demonstrates that the catalytic functions of the UDP-N-acetylglucosamine C4 epimerase WbpP and UDP-N-acetyl-D-glucosamine 6-dehydrogenase WbpA affect biofilm formation and lead to increased current density. Using optical coherence tomography, we found that the expression of each protein individually causes specific, quantifiable changes in biofilm architecture, including biovolume, height, and porosity. However, the current density did not significantly differ when these proteins were expressed alone compared to the control. In contrast, co-expression of WbpP and WbpA resulted in a doubling of current density, closely resembling the increases observed with riboflavin-mediated quorum sensing. We hypothesize that riboflavin-based quorum sensing may lead, through several intermediary steps, to the overproduction of WbpA and WbpP, resulting in better attachment to graphite anodes and thus higher current densities.

1. Introduction

Biofilm-based processes can offer significant advantages for various applications due to the resilience of cells within biofilms, the ease of separating the biocatalyst from the desired end product, and the high biomass densities achievable in biofilm systems [1,2]. Most of our knowledge about the physiology of microorganisms in biofilms comes from pathogenic species, driven by the serious problems these organisms and their biofilms can cause [3–6]. Conversely, the understanding of biofilm biocatalysts used in applied processes is relatively limited. Additionally, our knowledge of anaerobic biofilms remains largely unexplored, and it is uncertain whether findings from oxic conditions can be directly applied to anoxic systems.

Bioelectrochemical processes exemplify an application area for biofilms, where microorganisms form biofilms on the anodes or cathodes of electrochemical systems [2,7]. In these systems, the anode can serve as

* Corresponding author.
E-mail address: Johannes.gescher@tuhh.de (J. Gescher).
[1] 0000–0001-9642–0218
[2] 0009–0008-8400–176X
[3] 0000–0002-6174–7613
[4] 0000–0002-8631–1218
[5] 0009–0008-6283–0006
[6] 0000–0002-2708–0990
[7] 0000–0002-2963–2533
[8] 0000–0002-1625–8810

https://doi.org/10.1016/j.nbt.2025.05.006
Received 22 January 2025; Received in revised form 28 May 2025; Accepted 29 May 2025
Available online 9 June 2025

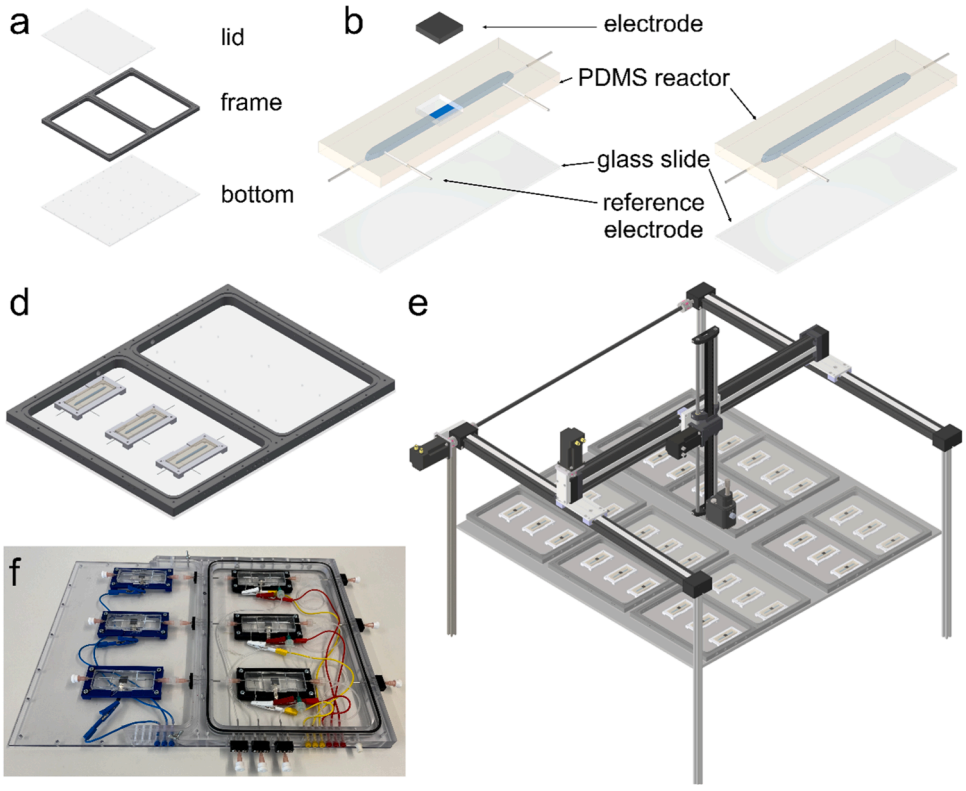

Fig. 1. Microfluidic biofilm cultivation platform. A microfluidic cultivation chamber consists of three parts: a lid, a frame and a bottom plate (a). The microfluidic reactors (b) are made of polydimethylsiloxane (PDMS) and the channel is sealed by plasma bonding to a glass slide. By the integration of a 1 × 1 cm graphite electrode, the reactor can be turned into a bioelectrochemical reactor. Further additional access points allow fluidic access via insertion of cannulas as well as the insertion of the tailored reference electrode. Two reactors are connected in series, where the first reactor serves as the anode (with the reference electrode), and the second reactor downstream functions as the cathode. This setup forms a complete bioelectrochemical system. Three triplicates fit into one chamber (d). The illustrated chamber is to be used for biofilm cultivation. In f a photo of a fully assembled chamber for bioelectrochemical cultivation can be seen. The microfluidic cultivation platform allows up to six triplicates to be operated simultaneously for continuous cultivation of biofilms (e). By integrating an optical coherence tomograph into a gantry robot, biofilm growth can be studied *in situ*. This setup and figure are based on the platform presented by Klein et al. [26] and were only slightly modified here.

an undepletable electron acceptor for microbes, while the cathode can act as an electron donor for the organisms. Two model organisms in the study of anode biofilms are *Shewanella oneidensis* and *Geobacter sulfurreducens*. *S. oneidensis* tends to form relatively thin biofilms on anodes, which may result from the lack of conductive structures in its extracellular polymeric substance (EPS) [8]. In contrast, *G. sulfurreducens* produces conductive nanowires that connect cells to one another and ultimately to the anode [8]. Consequently, biofilms comprising multiple cell layers are formed, which appear to be limited in activity due to a developing proton gradient characterized by low pH near the electrode surface [9].

Recently, Edel et al. [10] investigated the biofilm formation of the γ-proteobacterium *S. oneidensis* on anode surfaces. *S. oneidensis* is the most well-studied model organism regarding the transfer of respiratory electrons to electrode surfaces, using a network of *c*-type cytochromes to transport electrons from the cytoplasmic membrane to the cell surface [11–14]. The electron transport chain terminates almost directly at the surface of the outer membrane with the two decaheme cytochromes, MtrC and OmcA. Both cytochromes contain flavin cofactors that seem to facilitate electron transport through semiquinone formation [15–18]. Additionally, excess riboflavin in the medium (particularly under batch conditions) seems to be utilized for electron shuttling to nearby electron acceptors [19,20]. While the timing and mechanism of flavin cofactor binding to surface-bound cytochromes remain unclear, it has been established that FAD is transported into the periplasm via a specific transporter known as Bfe (bacterial flavin exporter) [21]. In the periplasm, at least some of the FAD is converted into FMN and AMP by the periplasmic 5′ nucleotidase UshA [22]. Beyond serving as a cofactor and electron shuttle, riboflavin acts as a quorum sensing molecule and enhances biofilm formation under anoxic conditions [10]. The concentration of external riboflavin regulates the expression of the ornithine decarboxylase (*speC*) in *S. oneidensis*, with increased levels of SpeC triggering enhanced biofilm formation. Although the mechanism behind SpeC-mediated biofilm formation remains unclear, it appears to occur at the post-transcriptional level. Notably, one of the proteins overproduced through SpeC overexpression is the UDP-N-acetylglucosamine C4 epimerase WbpP. Among the proteins significantly affected by SpeC, WbpP stands out as the only one with a known direct role in EPS formation, contributing to EPS production in various other species [23,24]. Nevertheless, WbpP was also shown to be involved in O-antigen synthesis in *Pseudomonas* strains [25]. If WbpP has a role in O-antigen or EPS formation in *S. oneidensis* is not clear yet. WbpP is localized in direct vicinity to WbpA, a UDP-N-acetyl-D-glucosamine 6-dehydrogenase, which could also have a function in both processes. The influence of WbpP and WbpA on anaerobic biofilm formation in *S. oneidensis* and their potential impact on current densities in bioelectrochemical systems have yet to be experimentally investigated.

To address this gap, we employed a recently developed biofilm analysis setup with microfluidic bioelectrochemical reactors [26] to analyze the effects of WbpP overexpression on anaerobic biofilm formation and current production. The study also incorporated WbpA, which is likely part of an operon with WbpP. Our analyses demonstrate that both proteins significantly alter biofilm architecture, but only their co-expression leads to a substantial increase in current density,

paralleling the increases observed with SpeC overexpression.

2. Materials and methods

2.1. Media and growth condition

All strains used in this study are listed in Table S1. *S. oneidensis* cells were pre-cultured overnight at 30 °C and 160 rpm in Lysogeny-Broth medium (LB) [27] and then transferred to minimal medium for microfluidic experiments. All media were prepared as described recently [28]. Media for strains carrying plasmids were always supplemented with 50 μg/mL kanamycin. For plasmid induction, the inoculum and culture media were supplemented with 100 μM arabinose.

For single-cell force spectroscopy, *S. oneidensis* cells were grown in LB medium with 100 μM arabinose at 30 °C until reaching the exponential phase. Strains containing pBad plasmids were maintained in the presence of kanamycin, and the expression of the *wbpAP* genes was induced using 100 μM arabinose, which was included in the medium for all experiments.

2.2. Construction of expression plasmid

The plasmid pBAD was utilized for the individual overexpression of the genes *wbpA* and *wbpP*, as well as for the co-overexpression of both genes. The plasmids were linearized using the restriction enzymes *Nco*I and *Pme*I. The *wbpA* and *wbpP* genes were amplified from the wild-type genome of *S. oneidensis*. Extended primers (see Table S2) were designed to introduce overlaps with the plasmid, enabling isothermal ligation as described by Gibson and colleagues [29]. The generated plasmids were verified by PCR analysis and subsequent sequencing.

2.3. Microfluidic biofilm cultivation platform

Biofilms were investigated using a newly developed microfluidic cultivation platform that operates under laminar flow conditions recently [26] (Fig. 1). The experimental conditions were the same as described recently [28].

2.4. Bioelectrochemical batch experiments

Bioelectrochemical batch experiments were performed in triplicate using a single-chamber system with a working volume of 270 mL [30]. Graphite felt (projected area of 36 cm^{-2}, SGL Group, Germany) and platinum mesh (projected area of 1.25 cm^{-2}, chemPUR, Germany) were used as working and counter electrode materials, respectively, and an Ag/AgCl electrode (Sensortechnik Meinsberg, Germany) served as a reference electrode. The entire BES setup was sterilized by autoclaving. The cells were pretreated as mentioned above and then resuspended to an OD_{600} of 0.07 in M4 medium containing 70 mM lactate. For chronoamperometric experiments, the working electrode was set to 0 mV vs. SHE and the current was monitored for 46 h. The BES setups were constantly flushed with N_2 gas to establish anoxic conditions. The medium was constantly stirred to mix it thoroughly.

2.5. Quantification of cells on anode felts

Cell quantification and quantitative polymerase chain reaction (qPCR) were conducted according to Edel et al. [10], without any modifications.

2.6. Optical coherence tomography (OCT)

Optical coherence tomography (OCT) is a non-invasive imaging technique that can be used to generate three-dimensional data sets of scattering materials, such as biofilms. To enable (semi-)automated OCT imaging, a gantry robot (DLE-RG-0003, igus® GmbH, Cologne, Germany) was used to capture images through the polycarbonate lids [26] (Fig. 1e). In this way, the development of the biofilm could be monitored throughout the experiment with high reproducibility and low workload. OCT images were acquired with a GanymedeTM spectral domain system (GAN611C1-SP1, Thorlabs GmbH, Dachau, Germany) and analyzed as described recently [26,28]. Based on the procedure developed by Wagner and Horn [31], height maps of the anodes were developed and surface roughness R_a was calculated from these images.

Table 1
Transcriptomic and proteomic analysis of *wbpA* and *wbpP*. The top part of the table shows the transcript per kilobase million (TPM) values of *wbpA* and *wbpP* from a transcriptome analysis of *Shewanella oneidensis* with and without the addition of riboflavin. Standard deviation was calculated from individual replicates (n = 2). The lower part of the table shows the intensity-based absolute quantification (iBAQ) values of a proteome analysis of *Shewanella oneidensis* with and without *speC* overexpression conditions. Standard deviation was calculated from individual replicates (n = 3). Moreover, the log2 fold change (L2FC) is given. This proteomic dataset was obtained from a previous study by Edel et al. [10] and was reanalyzed for the purposes of this study.

Transcriptomic Analysis			
Gene	**Riboflavin addition**	**No riboflavin addition**	
wbpA	375.06 ± 14.51	381.65 ± 23.55	
wbpP	281.56 ± 2.62	310.53 ± 31.13	
Proteomic Analysis			
Protein	***speC* overexpression**	**Wildtype**	**L2FC**
WbpA	8.05E+ 05 ± 1.02E+ 05	7.76E+ 05 ± 8.11E+ 04	0.05
WbpP	1.12E+ 05 ± 2.18E+ 04	4.81E+ 04 ± 7.35E+ 03	1.23

2.7. Transcriptomic analysis

Directional sequencing reads of comparative RNA-Sequences from Edel et al. [10], were analyzed with the CLC Genomics Workbench v20 using the RNA-Seq analysis workflow with standard parameters. Read mappings were visualized with representative reads in the region of interest for assessing the continuity of gene expression as an operon in one transcript.

2.8. Single-cell force spectroscopy

Substrate preparation, single-cell force spectroscopy and consecutive analysis of force distant curves was performed as described recently [28].

3. Results

3.1. wbpA and wbpP significantly alter biofilm characteristics

Recently Edel et al. have demonstrated that riboflavin functions similarly to a quorum sensing molecule in the γ-proteobacterium *S. oneidensis* [10]. The cells excrete riboflavin over time until a certain threshold concentration is reached, that seems to be below 37 nM. At or even below this concentration riboflavin triggers the overexpression of a single gene, *speC*, which encodes the ornithine decarboxylase. Its activity, in turn, leads apparently indirectly to biofilm production and enhanced current densities. In a proteomic study Edel and colleagues identified only a limited number of candidate proteins that were found to be differentially produced. Among the proteins significantly affected by SpeC, WbpP stands out as the only significantly upregulated protein that could directly catalyze chemical changes in the composition of the extracellular polymeric matrix (Table 1). This change in EPS chemistry could be the reason for the increased number of cells that were found to be attached to the anode of the bioelectrochemical system because of riboflavin-based quorum sensing. The UDP-N-acetylglucosamine C4 epimerase WbpP, was overproduced 1.23-fold compared to the control. WbpP has already been associated with biofilm formation in other

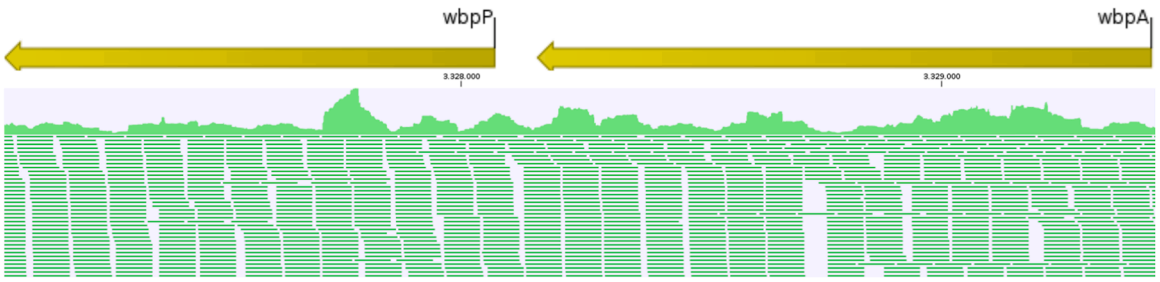

Fig. 2. Graphical representation of part of a transcriptomic analysis of *Shewanella oneidensis*. The mapped reads are shown as green lines in the region of the potential operon of *wbpA* and *wbpP*. The total coverage of the region is shown below the arrows indicating the coding sequences.

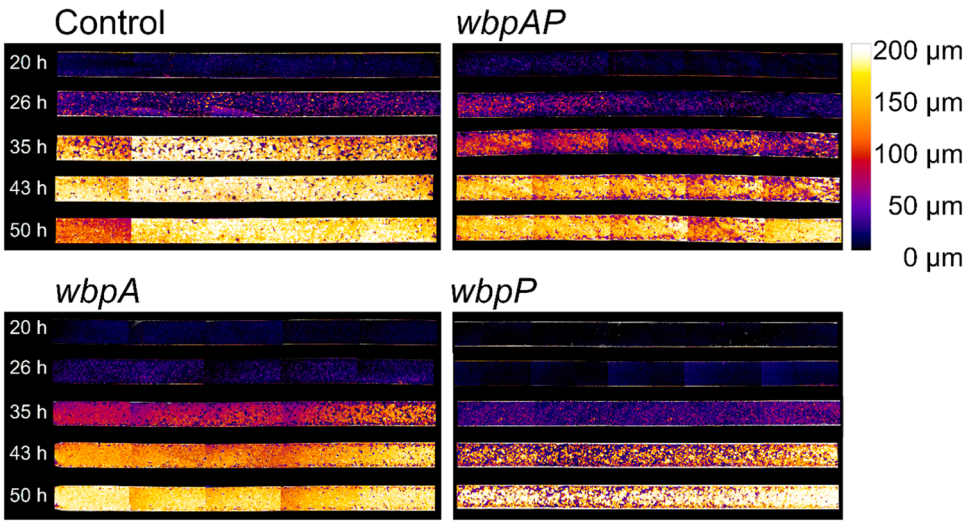

Fig. 3. Exemplary height maps of biofilms that were cultivated using microfluidic continuous flow reactors with lactate as electron donor and fumarate as electron acceptor. Cultivation was carried out under anoxic conditions and the retention time was 5.23 min at a flow rate of 4 mL h^{-1}. After 20, 26, 35, 43 and 50 h five images were taken of each cultivation channel, converted into color-coded height maps by processing and combined into one image by stitching. The cultivation channels shown have a size of 3 x 45 mm and a depth of 2 mm, corresponding to a top view of the biofilm, with flow direction from left to right. Cultivations were carried out in triplicate and the remaining height maps can be found in Fig. S1 in the supplement.

organisms [24,32]. In *S. oneidensis*, the corresponding gene appears to be in one operon together with *wbpA,* which encodes a UDP-N-acetyl-d-glucosamine 6-dehydrogenase. Although the proteomic study also indicated that the corresponding protein WbpA was slightly overproduced, the standard deviation ruled out statistical significance (Table 1). Examination of the transcriptomic data by Edel et al. [10] revealed coexpression of the two genes (Fig. 2). The TPM values for both genes differ by only 23 – 33 %, with the first gene in the operon *wbpA* showing higher expression than the subsequent *wbpP*, as expected. Mostly homogenous mapping of overlapping reads between the two genes reflects a continuous transcription in a single operon. To investigate the potential effects of the two proteins on biofilm formation and EPS production in *S. oneidensis*, *wbpP* and *wbpA* were expressed individually and together from an arabinose-inducible pBad plasmid.To systematically investigate the impact of overexpressing *wbpA*, *wbpP*, and the combination of both on biofilm formation, biofilms utilizing lactate as the electron donor and fumarate as the electron acceptor were examined within a microfluidic flow-through system. The development of the biofilm was monitored using integrated automated optical coherence tomography (OCT). Fig. 3 provides examples of height maps of the biofilms over time, presented as color-coded maps (remaining height maps can be found in Figure S1 in the supplement). Qualitatively the *wbpP*-overexpressing strain appears to form rougher biofilms generating thinner colonies that do not coalesce well into more homogeneous biofilm structures. In contrast, the *wbpA*-overexpressing strain seems to produce a smoother biofilm. Co-expression of both genes results in biofilm structures that exhibit characteristics that are intermediate between those formed by the individual gene overexpressions and a phenotype closely resembling that of the wild-type.

This qualitative observation is supported by quantitative data presented in Fig. 4 (Tables S3-6 in the supplement contain the mean values and standard deviations of Fig. 4). The WbpP strain consistently formed rougher biofilms throughout the entire experimental time course compared to the control and all other strains. The increased roughness became statistically significant at the last three time points of measurement. The *wbpA*-overexpressing strain demonstrated lower roughness compared to the control in four out of five measurements, with a significant difference observed at 43 h. The overproduction of both proteins together resulted in biofilms with roughness indices that were highly similar to the control. Additionally, after 50 h of cultivation, all mutants exhibited a significantly lower biovolume than the control, and a reduced biofilm height was observed after 35 h. At this point, substrate coverage was 100 % across all four strains. Biofilm porosity, which indicates the proportion of voids in the biofilm matrix also highlights differences between the strains. After 50 h, the *wbpA* and *wbpAP* overexpressing strains demonstrated significantly lower porosity. In contrast, the *wbpP* overexpressing strain produced more porous biofilms compared to the control at 35 and 43 h, but showed similar porosity to the control at the end of the experiment, after 50 h.

In summary, the individual overexpression strains formed structurally distinct biofilms compared to the control strain, while co-expression led to a phenotype that behaved similarly to the wild-type.

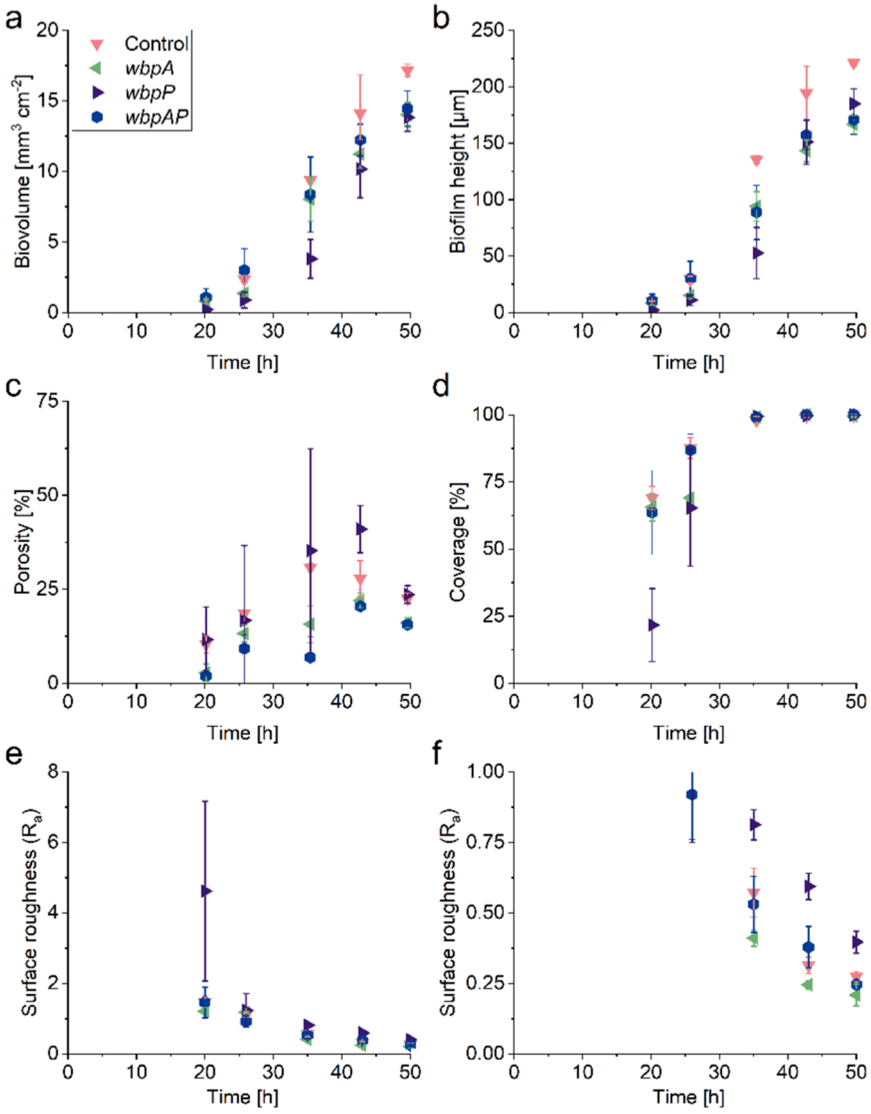

Fig. 4. Impact of the overexpression of *wbpA*, *wbpP* and *wbpAP* on biofilm development. Cultivation was conducted in microfluidic flow cells under anoxic conditions with lactate as electron donor and fumarate as electron acceptor. Biovolume (a), biofilm height (b), porosity (c), coverage (d) and surface roughness (e-f) are plotted over time. Error bars represent the standard deviation from individual replicates (n = 3). Tables S3-6 in the supplement contain the mean values and standard deviations of this figure.

3.2. Overexpression of wbpAP results in a significant increase in current density in bioelectrochemical continuous flow reactors

Microfluidic bioelectrochemical flowcells were used to investigate the influence of overexpression of *wbpA* and *wbpP* as well as a combination of both genes on current generation. As shown in Fig. 5, overexpression of either component had no effect on current generation under the conditions studied. However, overexpression of both genes together led to a significant 1.8-fold increase in current density compared to the control strain. Analysis of the current development over time indicates that the WbpAP overproducing strain exhibited a higher current density immediately after inoculation (inoculation is characterized by the high peak current densities from 0 to 3 h), which remained stable for the 48 h of the experiment. This suggests that a greater number of cells adhered to the anode surface right after inoculation, compared to the other strains tested. However, it was not possible to collect biofilm data as the ability of *S. oneidensis* to form anodic biofilms is rather limited [33–35] and the biofilm thickness was in the lowest range of the measurement sensitivity of the OCT device (8×8 x 5.5 µm). Hence, although we observe similar biofilm structures of the *wbpAP* overexpressing strain compared to the wildtype under fumarate reducing conditions the achievable current density is significantly higher. Of note, the peak current for all shown experiments is reached at the end of the inoculation (between 2 – 3 h). This can probably be attributed to the fact that *S. oneidensis* is a comparatively poor anodic biofilm-former with rather low current densities in flow-through setups. The peak most probably stems from the inoculated planktonic cells that depend on the anode as electron sink but eventually mostly get flushed out of the BES again. Similar behavior in flow-through setups has been observed in works from Klein and Wurst [26,36].

3.3. Overexpression of wbpAP impacts adhesion force and leads to higher cell densities on graphite anodes

The experiments conducted thus far have shown that only the overexpression of *wbpAP* leads to higher current densities in bioelectrochemical systems compared to all control strains. However, we were unable to observe a quantifiable difference in anaerobic biofilm formation when fumarate was used as the electron acceptor. This led us to investigate whether the attachment of cells to the anodes might have

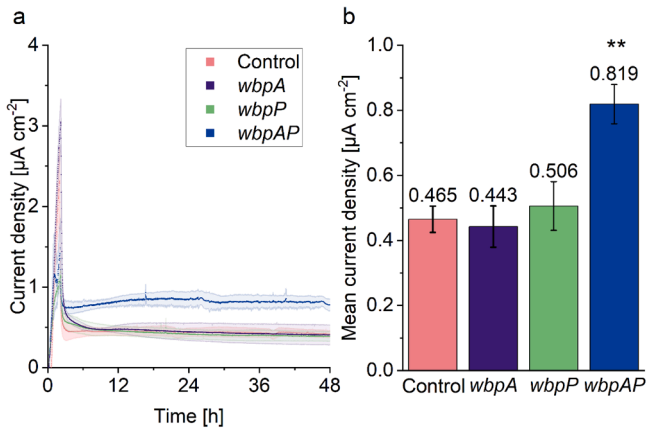

Fig. 5. Impact of overexpression of *wbpA*, *wbpP,* or *wbpAP* on mean current density in microfluidic bioelectrochemical flow reactors. Current development in the microfluidic bioelectrochemical systems over the whole time course of the experiment (a). Mean current densities (b). Error bars represent the standard deviation from individual replicates (n = 3). Asterisks represent significant differences to the control strain with the empty plasmid (unpaired *t*-test: ** = $p < 0.01$).

increased due to *wbpAP* overexpression. Since optical coherence tomography could not be used to assess biofilm growth on the electrodes, we aimed to determine if *wbpAP* overexpression resulted in altered cell numbers on the anodes using quantitative PCR (qPCR). Because the small size of the anodes in the microfluidic setups made quantitative assessments challenging, we conducted bioelectrochemical experiments in 250 mL setups with larger graphite felt electrodes. The systems were operated for 46 h, during which the *wbpAP*-overexpressing strain produced 1.45 times more current (unpaired *t*-test: $p < 0.01$). While this difference is slightly smaller than that observed in the microfluidic system, it can be most likely attributed to the batch operation, where planktonic cells can also contribute to current production.

Quantitative PCR (qPCR) analysis indicated that 1.97 ± 0.22 times more *wbpAP*-expressing cells were detected on the electrodes compared to the control. Additionally, we sought to determine whether the observed increase in cell density on the electrodes due to *wbpAP* overexpression could be traced to the level of individual cells. Therefore, we conducted single-cell force spectroscopy on wild-type, control cells containing an empty pBAD plasmid, and *wbpAP*-overexpressing cells on smooth hydrophobic surfaces resembling the graphite material (Fig. 6). Both the wild-type and control strains exhibited similar adhesion force results, suggesting that the presence of the plasmid and the addition of kanamycin did not significantly alter the surface chemistry of the cells. In contrast, the *wbpAP*-overexpressing strain demonstrated a shift toward lower adhesion strength, which may be due to increased surface hydrophilicity resulting from WbpAP activity. (fig.7)

4. Discussion

In particular, the ability of *S. oneidensis* to form only very thin biofilms is often seen as the reason for the low current densities that can be achieved in comparison to the other exoelectrogenic model organism *G. sulfurreducens* [37–39]. Biofilm formation by *S. oneidensis* is well studied under oxic conditions [10,40–43] but interestingly, knowledge of biofilm formation by *S. oneidensis* and other strains of this genus under anoxic conditions is rather sparse, and it is generally assumed that wild-type strains form only thin or single-layer biofilms under anoxic conditions. Our experiments did not confirm the general inability of *S. oneidensis* to form biofilms in the absence of oxygen, as biofilms thicker than 200 µm could be formed with fumarate as electron acceptor.

The experiments suggest that the catalytic functions of WbpA and WbpP alter the properties of the biofilm. As illustrated in Fig. 8, WbpA (SO*3190)* is a UDP-N-acetyl-D-glucosamine 6-dehydrogenase that catalyzes the conversion of UDP-N-acetyl-D-galactosamine (UDP-GalNAc) to UDP-N-acetyl-D-galactosaminuronic acid (UDP-GalNAcA) and UDP-N-acetyl-D-glucosamine (UDP-GlcNAc) to UDP-N-acetyl-D-glucosaminuronic acid (UDP-GlcNAcA). WbpP (SO3189) functions as a UDP-N-acetylglucosamine C4 epimerase, catalyzing the reactions that transform UDP-GlcNAc into UDP-GalNAc and UDP-GlcNAcA into UDP-GalNAcA. Both GlcNAc and GalNAc are common exopolysaccharides found in microbial extracellular matrices [44,45]. Nevertheless, both proteins may also influence the biochemistry of the organism's O-antigen. Localized upstream of WbpA are the genes *wza*, *wzd*, and *wzz*. The *wza* gene encodes a polysaccharide export protein that plays a role in both O-antigen and capsule biosynthesis, while *wzz* encodes a protein that regulates the chain length of the O-antigen. In contrast, Wzd has been annotated as a protein involved in capsular biosynthesis. In *Streptococcus pneumoniae*, Wzd has been shown to be important for capsule coverage over the septum during cell division, interacting with

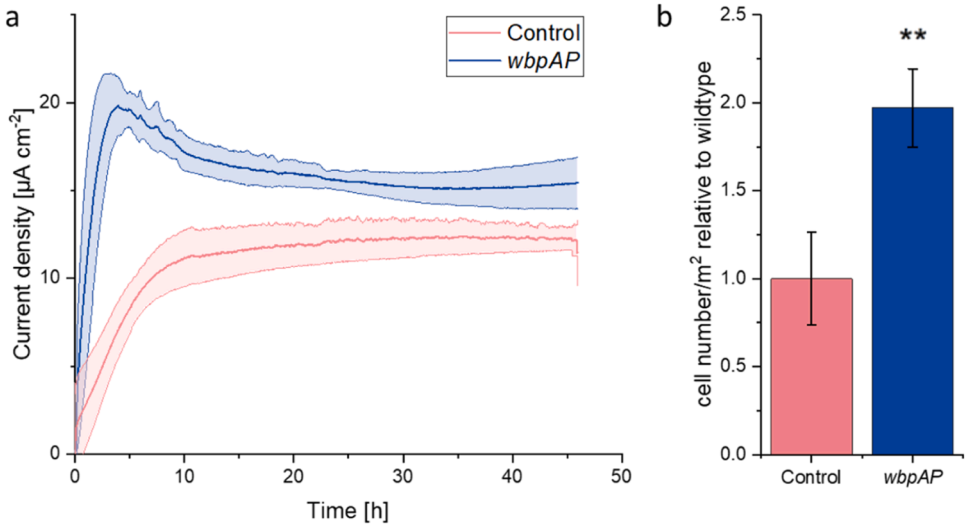

Fig. 6. Impact of overexpression of *wbpAP* on current density and cell number in microbial electrolysis cells under batch conditions. Current development in the bioelectrochemical system over the whole time course of the experiment (a). Cell number evaluated using qPCR (b). Error bars represent the standard deviation from individual replicates (n = 3). Asterisks represent significant differences to the control strain with the empty plasmid (unpaired *t*-test: ** = $p < 0.01$).

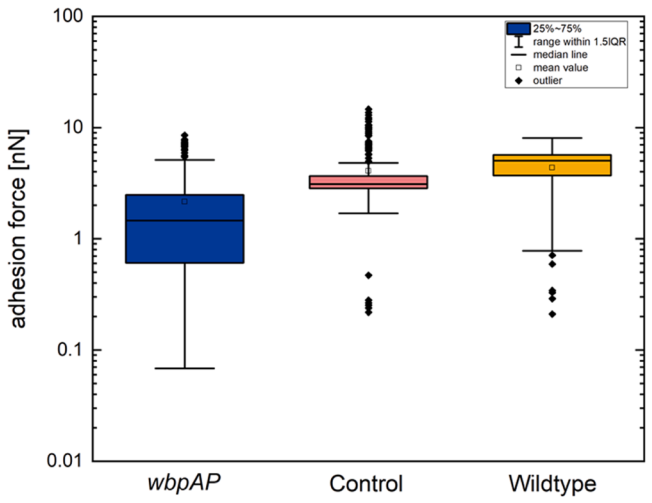

Fig. 7. Statistical min-to-max box plots of the adhesion force for different *S. oneidensis* variants on OTS. For every variant the median line (blackline in the box), the mean value (empty square) and the outlier (black rhombs) is shown. Three individual cells were measured for every variant. To receive the boxplots all countable adhesion events of each bacterial cell were summed up.

Wze in this process [46]. Wze, does not seem to be part of the gen-ecluster in *S. oneidensis*. Downstream of *wbpP* are several additional genes encoding proteins potentially involved in polysaccharide and O-antigen biosynthesis, including the O-antigen flippase *wzx* and O-antigen polymerase *wzy* [47]. Therefore, we suggest that the function of WbpAP may be involved at least not only in capsule but also in O-antigen biosynthesis. O-antigen biochemistry will probably be a major determining function for initial cell-cell interaction before the biofilm matures over time.

Regarding the structure of biofilms grown with lactate and fumarate, the catalytic action of WbpA appears to lead to more uniform biofilms. The porosity of biofilms from WbpA- and WbpAP-overproducing cells is lower than that of the control strain and the strain expressing only WbpP. Also the roughness of biofilms from WbpA expressing cells is at least at one time point significantly lower compared to the control. This reduced porosity may result from increased polarity of the cell surface due to the oxidation of a hydroxyl group to the corresponding carboxylic acid. Conversely, the expression of WbpP alone seems to have the most pronounced effects on biofilm structure, resulting in significantly higher porosity at 35 and 50 h compared to all other characterized strains, as well as increased surface roughness between these time points. To our knowledge, this study is the first to analyze the influence of sugar stereochemistry on biofilm formation. The findings suggest that epimerization can act as a key regulator in altering biofilm architecture.

When an anode is used as the sole terminal electron acceptor, *Shewanella* appears unable to form multilayer biofilms. The biofilm thickness under electrode-respiring conditions fell below the detection limit of optical coherence tomography (OCT), preventing the establishment of any correlations between biofilm architecture and current density. However, the simultaneous overexpression of *wbpA* and *wbpP* resulted in a 1.8-fold increase in current density within the continuously operated microfluidic system. The biofilms of this mutant strain exhibited reduced height and porosity under fumarate-respiring conditions when compared to both the control and the strain expressing only *wbpP*. This suggests that *wbpA* expression leads to the formation of denser biofilms. Interestingly, the increased current production associated with *wbpA* overexpression did not occur independently; the activity of the epimerase WbpP was also required. Notably, the observed boost in current production following the overexpression of *wbpAP* closely resembles the increase seen with overexpression of *speC* alone in a previous study (1.9-fold versus 1.8-fold, respectively). This correlation suggests that the *speC*-driven production of WbpAP may underlie the riboflavin-based quorum sensing enhancement of current density. However, the exact mechanism through which both epimerization and oxidation—catalyzed by WbpP and WbpA, respectively—must occur simultaneously to achieve this effect remains unclear.

Changing the surface chemistry of the cells will likely affect their hydrophilicity. Of note, whether stronger hydrophobicity or stronger hydrophilicity encourages better cell adhesion and biofilm formation seems highly debated and dependent on the organism, probably even dependent on the strains being used, with publications tending towards both directions [48–52]. Experiments aiming at quantifying adhesion forces indicate that *wbpAP* overexpression leads to lower adhesion forces on a hydrophobic biofilm substratum compared to the control strain. The lower interaction with hydrophobic surfaces could also imply that

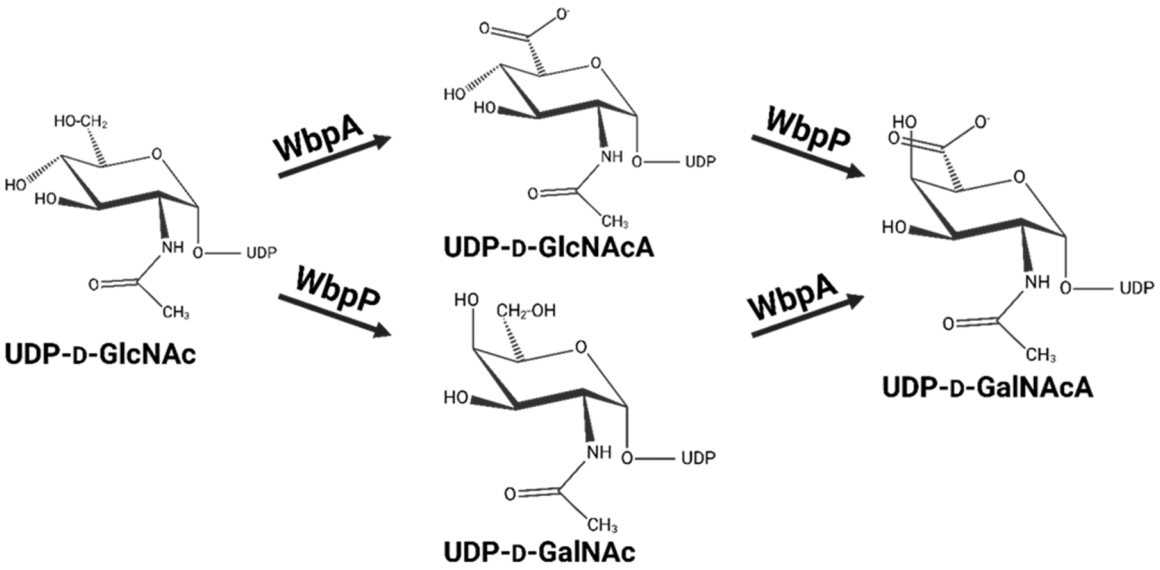

Fig. 8. Reactions catalyzed by WbpA and WbpP in *Shewanella oneidensis*. WbpA (SO_3190) is UDP-N-acetyl-d-glucosamine 6-dehydrogenase, which catalyzes the reaction of UDP-N-acetyl-D-galactosamine (UDP-GalNAc) to UDP-N-acetyl-D-galactosaminuronic acid (UDP-GalNAcA) and UDP-N-acetyl-D-glucosamine (UDP-GlcNAc) to UDP-N-acetyl-D-glucosaminuronic acid (UDP-GlcNAcA). WbpP (SO_3189) is a UDP-N-acetylglucosamine C4 epimerase that catalyzes the reactions of UDP-GlcNAc to UDP-GalNAc and UDP-GlcNAcA to UDP-GalNAcA.

the interactions between the comparably hydrophilic cells are more robust. In this case, it could be possible that the contact between individual cells also on the surface of the electrode could be closer which might lead to a more effective cell-cell electron transfer supporting cell metabolism even if direct contact to the electrode is not possible. Also, the biofilm might be more robust regarding shear forces. As *S. oneidensis* does not form multilayered biofilms on electrode surfaces this effect cannot lead to dramatic cell number and current increases which is in line with the observed 2-fold and 1.8-fold increase in cell number and current density, respectively. Still, further research will be necessary to investigate cell-to-cell adhesion forces especially also between cells overexpressing only *wbpA* and *wbpAP* as only *wbpAP* expression led to the observed increase in current density, a characteristic that we cannot explain so far.

Experiments aiming at quantifying adhesion forces indicate that *wbpAP* overexpression leads to lower adhesion forces on a hydrophobic biofilm substrate. This reduced adhesion may stem from increased hydrophilicity primarily due to WbpA activity. Nonetheless, lower interaction with hydrophobic surfaces could also imply that the interactions between hydrophilic cells are more robust. Further research will be necessary to investigate cell-to-cell adhesion forces.

Moreover, since the fumarate-respiring experiments showed a lowered porosity for the *wbpAP* and *wbpA* overexpressing strain, it can be expected that the cell density on an anode is higher compared to the control because there are less uncolonized voids on the electrode. Lower porosity also means closer cell-cell contact and therefore better adhesion among cells, leading to more cells per area. This is in line with the adhesion force experiments and qPCR results, that showed a lower hydrophobicity and therefore an increased hydrophilicity. It may seem counterintuitive that a lower hydrophobicity results in more biomass on a hydrophobic graphite anode, so this has to be attributed to a better cell-cell adhesion, leading to an overall higher cell number on the electrode. Whether stronger hydrophobicity or stronger hydrophilicity encourages better cell adhesion and biofilm formation seems highly debated and dependent on the organism, probably even dependent on the strains being used, with publications tending towards both directions [48–52].

So far, several studies showed that extracellular polymeric matrix components can have a current limiting effect. Kouzuma and colleagues discovered that disruption of the gene SO3177 which is involved in capsule biosynthesis can lead to an increase in current density which was correlated to less EPS production and a more hydrophobic cell surface [53]. Bursac et al. revealed that deletion of the λ prophage can lead to increased current which is likely correlated with a decrease in extracellular DNA content [54]. Moreover, Gao et al. could reveal that shearing off the EPS matrix of *Shewanella* cells leads to cells catalyzing superior electron transfer kinetics compared to the natural control strain [55]. This study represents one of the few instances where engineering the expression of genes involved in extracellular sugar chemistry has been successfully employed to tailor current density in bioelectrochemical systems. Most previous attempts have focused on altering the expression of protein components within the EPS to enhance cell-cell interactions [56]. The production of EPS is highly complex, and the chemistry of EPS polymers remains incompletely understood. We hope this study marks the beginning of a comprehensive assessment of how EPS chemistry influences applied biofilm processes and the potential to enhance biofilm performance in practical applications through the control of EPS chemistry.

Ethics

This article does not contain any studies with human participants or animals performed by any of the authors.

Funding

This study was funded by the project “Continuous Bioproduction Using a Tailored Biocatalyst for Electrode Assisted Fermentation” (grant number 031B0847C) of the Federal Ministry of Education and Research (BMBF), the project “Synthetic engineering of conductive biofilm development in the γ-proteobacterium *Shewanella oneidensis*” of the German Research Foundation (DFG), and the DFG large instrument funding under grant number INST 256/542–1 FUGG (project number 449375068).

CRediT authorship contribution statement

René Wurst: Writing – review & editing, Validation. **Christian Jonas Lapp:** Visualization. **Edina Marlen Klein:** Writing – review & editing, Writing – original draft, Visualization, Validation, Methodology, Investigation, Formal analysis, Data curation, Conceptualization. **Hannah Heintz:** Writing – review & editing, Visualization, Methodology, Investigation, Formal analysis. **Johannes Gescher:** Writing – review & editing, Writing – original draft, Validation, Supervision, Resources, Project administration, Methodology, Funding acquisition, Conceptualization. **Hendrik Hähl:** Writing – review & editing, Visualization, Supervision, Methodology, Formal analysis. **Karin Jacobs:** Writing – review & editing, Supervision, Resources, Project administration, Funding acquisition, Data curation, Conceptualization. **Miriam Edel:** Investigation.

Declaration of Competing Interest

The authors declare that they have no known competing financial interests or personal relationships that could have appeared to influence the work reported in this paper

Acknowledgements

This work was financially supported from the projects “Continuous Bioproduction Using a Tailored Biocatalyst for Electrode Assisted Fermentation” (grant no: 031B0847C) of the Federal Ministry of Education and Research (BMBF) and “Synthetic engineering of conductive biofilm development in the γ-proteobacterium *Shewanella oneidensis*“ of the German Research Foundation (DFG). The authors H.H., H.H. and K. J. thank the German Research Foundation (DFG) for funding within the Collaborative Research Center SFB 1027. This research was also supported by DFG large instrument funding under grant number INST 256/542–1 FUGG (project number 449375068). K.J. would like to thank the German Federal Ministry of Education and Research (BMBF) for their support of the Max Planck School Matter to Life in collaboration with the Max Planck society.

Appendix A. Supporting information

Supplementary data associated with this article can be found in the online version at doi:10.1016/j.nbt.2025.05.006.

Data availability

Data will be made available on request.

References

[1] Edel M, Horn H, Gescher J. Biofilm systems as tools in biotechnological production. Appl Microbiol Biotechnol 2019;103:5095–103. https://doi.org/10.1007/s00253-019-09869-x.

[2] Klein EM, Knoll MT, Gescher J. Microbe–Anode Interactions: Comparing the impact of genetic and material engineering approaches to improve the performance of microbial electrochemical systems (MES). Micro Biotechnol 2023;16:1179–202. https://doi.org/10.1111/1751-7915.14236.

[3] Høiby N, Bjarnsholt T, Moser C, Bassi GL, Coenye T, Donelli G, et al. ESCMID guideline for the diagnosis and treatment of biofilm infections 2014. Clin Microbiol Infect 2014;21:1–25. https://doi.org/10.1016/J.CMI.2014.10.024.

[4] Lebeaux D, Chauhan A, Rendueles O, Beloin C. From *in vitro* to *in vivo* Models Of Bacterial Biofilm-related Infections. Pathogens 2013;2:288. https://doi.org/10.3390/PATHOGENS2020288.

[5] Vestby LK, Grønseth T, Simm R, Nesse LL. Bacterial biofilm and its role in the pathogenesis of disease. Antibiotics 2020;9:59. https://doi.org/10.3390/ANTIBIOTICS9020059.

[6] Srinivasan R, Santhakumari S, Poonguzhali P, Geetha M, Dyavaiah M, Xiangmin L. Bacterial biofilm inhibition: a focused review on recent therapeutic strategies for combating the biofilm mediated infections. Front Microbiol 2021;12:676458. https://doi.org/10.3389/fmicb.2021.676458.

[7] Greenman J, Gajda I, You J, Mendis BA, Obata O, Pasternak G, et al. Microbial fuel cells and their electrified biofilms. Biofilm 2021;3:100057. https://doi.org/10.1016/J.BIOFLM.2021.100057.

[8] Lovley DR, Walker DJF. Geobacter protein nanowires. Front Microbiol 2019;10:474567. https://doi.org/10.3389/fmicb.2019.02078.

[9] Torres CI, Marcus AK, Rittmann BE. Proton transport inside the biofilm limits electrical current generation by anode-respiring bacteria. Biotechnol Bioeng 2008;100:872–81. https://doi.org/10.1002/BIT.21821.

[10] Edel M, Sturm G, Sturm-Richter K, Wagner M, Ducassou JN, Couté Y, et al. Extracellular riboflavin induces anaerobic biofilm formation in *Shewanella oneidensis*. Biotechnol Biofuels 2021;14:130. https://doi.org/10.1186/S13068-021-01981-3.

[11] Simonte F, Sturm G, Gescher J, Sturm-Richter K. Extracellular electron transfer and biosensors. Adv Biochem Eng Biotechnol 2019;167:15–38. https://doi.org/10.1007/10_2017_34.

[12] Edwards MJ, Richardson DJ, Paquete CM, Clarke TA. Role of multiheme cytochromes involved in extracellular anaerobic respiration in bacteria. Protein Sci 2020;4:830–42. https://doi.org/10.1002/PRO.3787.

[13] Richter K, Schicklberger M, Gescher J. Dissimilatory reduction of extracellular electron acceptors in anaerobic respiration. Appl Environ Microbiol 2012;78:913–21. https://doi.org/10.1128/AEM.06803-11.

[14] Breuer M, Rosso KM, Blumberger J, Butt JN. Multi-haem cytochromes in *Shewanella oneidensis* MR-1: structures, functions and opportunities. J R Soc Interface 2015;12:20141117. https://doi.org/10.1098/rsif.2014.1117.

[15] Xu S, Jangir Y, El-Naggar MY. Disentangling the roles of free and cytochrome-bound flavins in extracellular electron transport from *Shewanella oneidensis* MR-1. Electro Acta 2016;198:49–55. https://doi.org/10.1016/J.ELECTACTA.2016.03.074.

[16] Okamoto A, Hashimoto K, Nealson KH, Nakamura R. Rate enhancement of bacterial extracellular electron transport involves bound flavin semiquinones. Proc Natl Acad Sci USA 2013;110:7856–61. https://doi.org/10.1073/pnas.1220823110.

[17] Okamoto A, Nakamura R, Nealson KH, Hashimoto K. Bound flavin model suggests similar electron-transfer mechanisms in *Shewanella* and *Geobacter*. ChemElectroChem 2014;1:1808–12. https://doi.org/10.1002/CELC.201402151.

[18] Okamoto A, Saito K, Inoue K, Nealson KH, Hashimoto K, Nakamura R. Uptake of self-secreted flavins as bound cofactors for extracellular electron transfer in *Geobacter* species. Energy Environ Sci 2014;7:1357–61. https://doi.org/10.1039/C3EE43674H.

[19] Von Canstein H, Ogawa J, Shimizu S, Lloyd JR. Secretion of flavins by *Shewanella* species and their role in extracellular electron transfer. Appl Environ Microbiol 2008;74:615–23. https://doi.org/10.1128/AEM.01387-07.

[20] Marsili E, Baron DB, Shikhare ID, Coursolle D, Gralnick JA, Bond DR. *Shewanella* secretes flavins that mediate extracellular electron transfer. Proc Natl Acad Sci USA 2008;105:3968–73. https://doi.org/10.1073/pnas.0710525105.

[21] Kotloski NJ, Gralnick JA. Flavin electron shuttles dominate extracellular electron transfer by *Shewanella oneidensis*. MBio 2013;4:553–65. https://doi.org/10.1128/MBIO.00553-12.

[22] Covington ED, Gelbmann CB, Kotloski NJ, Gralnick JA. An essential role for UshA in processing of extracellular flavin electron shuttles by *Shewanella oneidensis*. Mol Microbiol 2010;78:519–32. https://doi.org/10.1111/J.1365-2958.2010.07353.X.

[23] Lee KJ, Kim JA, Hwang W, Park SJ, Lee KH. Role of capsular polysaccharide (CPS) in biofilm formation and regulation of CPS production by quorum-sensing in *Vibrio vulnificus*. Mol Microbiol 2013;90:841–57. https://doi.org/10.1111/MMI.12401.

[24] Park NY, Lee JH, Kim MW, Jeong HG, Lee BC, Kim TS, et al. Identification of the *Vibrio vulnificus wbpP* gene and evaluation of its role in virulence. Infect Immun 2006;74:721–8. https://doi.org/10.1128/IAI.74.1.721-728.2006.

[25] Lam JS, Taylor VL, Islam ST, Hao Y, Kocíncová D. Genetic and functional diversity of *Pseudomonas aeruginosa* lipopolysaccharide. Front Microbiol 2011;2:10831. https://doi.org/10.3389/fmicb.2020.598478.

[26] Klein EM, Wurst R, Rehnlund D, Gescher J. Elucidating the development of cooperative anode-biofilm-structures. Biofilm 2024;7:100193. https://doi.org/10.1016/j.bioflm.2024.100193.

[27] Lennox ES. Transduction of linked genetic characters of the host by bacteriophage P1. Virology 1955;1:190–206. https://doi.org/10.1016/0042-6822(55)90016-7.

[28] Klein EM, Heintz H, Wurst R, Schuldt S, Hähl H, Jacobs K, et al. Comparative analysis of the influence of BpfA and BpfG on biofilm development and current density in *Shewanella oneidensis* under oxic, fumarate- and anode-respiring conditions. Sci Rep 2024;14:23174. https://doi.org/10.1038/s41598-024-73474-w.

[29] Gibson DG, Young L, Chuang RY, Venter JC, Hutchison CA, Smith HO. Enzymatic assembly of DNA molecules up to several hundred kilobases. Nat Methods 2009;6(5):343. https://doi.org/10.1038/NMETH.1318.

[30] Knoll MT, Fuderer E, Gescher J. Sprayable biofilm – Agarose hydrogels as 3D matrix for enhanced productivity in bioelectrochemical systems. Biofilm 2022;4:100077. https://doi.org/10.1016/J.BIOFLM.2022.100077.

[31] Wagner M, Horn H. Optical coherence tomography in biofilm research: a comprehensive review. Biotechnol Bioeng 2017;114:1386–402. https://doi.org/10.1002/BIT.26283.

[32] Niou YK, Wu WL, Lin LC, Yu MS, Shu HY, Yang HH, et al. Role of *galE* on biofilm formation by *Thermus* spp. Biochem Biophys Res Commun 2009;390:313–8. https://doi.org/10.1016/J.BBRC.2009.09.120.

[33] Baron D, LaBelle E, Coursolle D, Gralnick JA, Bond DR. Electrochemical measurement of electron transfer kinetics by *Shewanella oneidensis* MR-1. J Biol Chem 2009;284:28865–73. https://doi.org/10.1074/jbc.M109.043455.

[34] Kitayama M, Koga R, Kasai T, Kouzuma A, Watanabe K. Structures, compositions, and activities of live *Shewanella* biofilms formed on graphite electrodes in electrochemical flow cells. Appl Environ Microbiol 2017;83:e00903–17. https://doi.org/10.1128/AEM.00903-17.

[35] Rosenbaum MA, Bar HY, Beg QK, Segrè D, Booth J, Cotta MA, et al. Transcriptional analysis of *Shewanella oneidensis* MR-1 with an electrode compared to Fe(III)citrate or oxygen as terminal electron acceptor. PLoS One 2012;7:e30827. https://doi.org/10.1371/JOURNAL.PONE.0030827.

[36] Wurst R, Klein EM, Gescher J. Magnetic, conductive nanoparticles as building blocks for steerable micropillar-structured anodic biofilms. Biofilm 2024;8:100226. https://doi.org/10.1016/J.BIOFLM.2024.100226.

[37] Erben J, Pinder ZA, Lüdtke MS, Kerzenmacher S. Local acidification limits the current production and biofilm formation of *Shewanella oneidensis* MR-1 with electrospun anodes. Front Microbiol 2021;12:660474. https://doi.org/10.3389/fmicb.2021.660474.

[38] Liu T, Yu YY, Deng XP, Ng CK, Cao B, Wang JY, et al. Enhanced *Shewanella* biofilm promotes bioelectricity generation. Biotechnol Bioeng 2015;112:2051–9. https://doi.org/10.1002/BIT.25624.

[39] Lanthier M, Gregory KB, Lovley DR. Growth with high planktonic biomass in *Shewanella oneidensis* fuel cells. FEMS Microbiol Lett 2008;278:29. https://doi.org/10.1111/J.1574-6968.2007.00964.X.

[40] Thormann KM, Saville RM, Shukla S, Pelletier DA, Spormann AM. Initial phases of biofilm formation in *Shewanella oneidensis* MR-1. J Bacteriol 2004;186:8096. https://doi.org/10.1128/JB.186.23.8096-8104.2004.

[41] Thormann KM, Duttler S, Saville RM, Hyodo M, Shukla S, Hayakawa Y, et al. Control of formation and cellular detachment from *Shewanella oneidensis* MR-1 biofilms by cyclic di-GMP. J Bacteriol 2006;188:2681–91. https://doi.org/10.1128/jb.188.7.2681-2691.2006.

[42] Teal TK, Lies DP, Wold BJ, Newman DK. Spatiometabolic stratification of *Shewanella oneidensis* biofilms. Appl Environ Microbiol 2006;72:7324–30. https://doi.org/10.1128/AEM.01163-06.

[43] Liang Y, Gao H, Chen J, Dong Y, Wu L, He Z, et al. Pellicle formation in *Shewanella oneidensis*. BMC Microbiol 2010;10:1–11. https://doi.org/10.1186/1471-2180-10-291.

[44] Vandana SDas. Genetic regulation, biosynthesis and applications of extracellular polysaccharides of the biofilm matrix of bacteria. Carbohydr Polym 2022;291:119536. https://doi.org/10.1016/J.CARBPOL.2022.119536.

[45] Flemming HC, Neu TR, Wingender J. The perfect slime: microbial extracellular polymeric substances (EPS). Water Intell Online 2016;15. 9781780407425.

[46] Figueiredo J, Henriques MX, Catalão MJ, Pinheiro S, Narciso AR, Mesquita F, et al. Encapsulation of the septal cell wall protects *Streptococcus pneumoniae* from its major peptidoglycan hydrolase and host defenses. PLoS Pathog 2022;18:e1010516. https://doi.org/10.1371/JOURNAL.PPAT.1010516.

[47] Aydanian A, Tang L, Morris JG, Johnson JA, Stine OC. Genetic diversity of O-antigen biosynthesis regions in *Vibrio cholerae*. Appl Environ Microbiol 2011;77:2247–53. https://doi.org/10.1128/AEM.01663-10.

[48] van Oss CJ. Hydrophobicity and hydrophilicity of biosurfaces. Curr Opin Colloid Interface Sci 1997;2:503–12. https://doi.org/10.1016/S1359-0294(97)80099-4.

[49] De-la-Pinta I, Cobos M, Ibarretxe J, Montoya E, Eraso E, Guraya T, et al. Effect of biomaterials hydrophobicity and roughness on biofilm development. J Mater Sci Mater Med 2019;30:77. https://doi.org/10.1007/S10856-019-6281-3.

[50] Zhu J, Wang M, Zhang H, Yang S, Song KY, Yin R, et al. Effects of hydrophilicity, adhesion work, and fluid flow on biofilm formation of PDMS in microfluidic systems. ACS Appl Bio Mater 2020;3:8386–94.

[51] Guo K, Freguia S, Dennis PG, Chen X, Donose BC, Keller J, et al. Effects of surface charge and hydrophobicity on anodic biofilm formation, community composition, and current generation in bioelectrochemical systems. Environ Sci Technol 2013;47:7563–70.

[52] Boks NP, Norde W, van der Mei HC, Busscher HJ. Forces involved in bacterial adhesion to hydrophilic and hydrophobic surfaces. Microbiology 2008;154:3122–33. https://doi.org/10.1099/MIC.0.2008/018622-0.

[53] Kouzuma A, Meng XY, Kimura N, Hashimoto K, Watanabe K. Disruption of the putative cell surface polysaccharide biosynthesis Gene SO3177 in *Shewanella oneidensis* MR-1 enhances adhesion to electrodes and current generation in microbial fuel cells. Appl Environ Microbiol 2010;76:4151–7. https://doi.org/10.1128/AEM.00117-10.

[54] Bursac T, Gralnick JA, Gescher J. Acetoin production via unbalanced fermentation in *Shewanella oneidensis*. Biotechnol Bioeng 2017;114:1283–9. https://doi.org/10.1002/bit.26243.

[55] Gao L, Lu X, Liu H, Li J, Li W, Song R, et al. Mediation of extracellular polymeric substances in microbial reduction of hematite by *Shewanella oneidensis* MR-1. Front Microbiol 2019;10:437935. https://doi.org/10.3389/fmicb.2019.00575.

[56] Zhao F, Chavez MS, Naughton KL, Niman CM, Atkinson JT, Gralnick JA, et al. Light-induced patterning of electroactive bacterial biofilms. ACS Synth Biol 2022; 11:2327–38. https://doi.org/10.1021/acssynbio.2c00024.